PHYSICAL REVIEW LETTERS

Observation of Thermoelectric Currents in High-Field Superconductor-Ferromagnet Tunnel Junctions

S. Kolenda, M. J. Wolf,[*] and D. Beckmann[†]
Institute of Nanotechnology, Karlsruhe Institute of Technology, Karlsruhe, Germany
(Received 18 September 2015; revised manuscript received 17 December 2015; published 1 March 2016)

We report on the experimental observation of spin-dependent thermoelectric currents in superconductor-ferromagnet tunnel junctions in high magnetic fields. The thermoelectric signals are due to a spin-dependent lifting of the particle-hole symmetry, and are found to be in excellent agreement with recent theoretical predictions. The maximum Seebeck coefficient inferred from the data is about $-100 \ \mu$V/K, much larger than commonly found in metallic structures. Our results directly prove the coupling of spin and heat transport in high-field superconductors.

Spin-dependent transport properties of superconductor hybrid structures have attracted considerable interest recently with the discovery of long-range triplet supercurrents [1–3], long quasiparticle spin lifetimes [4], and the quasiparticle spin Hall effect [5]. A particularly interesting system is superconductors with a spin splitting of the density of states, which enables long-range quasiparticle spin transport [6–9], superconducting magnetic tunnel junctions [10], and the observation of quasiparticle electron spin resonance [11] at high fields. The coupling of spin and charge transport in superconductor hybrid structures, and the search for possible functional devices, is now commonly called superconducting spintronics [12,13]. The coupling of charge and heat transport in nanoscale superconductor hybrid structures is an active field of current research due to applications as thermometers, microrefrigerators, and particle detectors [14,15]. Superconductor hybrid structures exhibit phase-coherent thermoelectric effects in Andreev interferometers [16] and heat interferometry in Josephson junctions [17,18], and advances in nanofabrication have shed new light on the old question of thermoelectric magnetic flux in bimetallic superconducting rings [19]. The coupling of spin and heat currents in normal-metal–ferromagnet devices leads to spin-dependent Seebeck [20] and Peltier [21] effects, which have spawned the field of spin caloritronics [22]. It has recently been proposed that large spin-dependent thermoelectric effects occur in superconductor-ferromagnet hybrid structures [23–27]. These may lead to improved devices similar to normal-state spin caloritronics such as local thermometers [28] and coolers with a thermoelectric figure of merit $ZT > 1$ [24,25], but also qualitatively different device concepts such as phase-coherent thermoelectric transistors [29–31]. Also, it has been proposed that long-range spin transport in high-field superconductors is actually coupled to heat currents [32–35], but this has not yet been shown directly. Here, we report on the direct experimental observation of spin-dependent thermoelectric effects in

superconductor-ferromagnet hybrid structures, where spin polarized currents are driven by thermal rather than electric excitation.

Thermoelectric effects in metals are caused by the broken symmetry between electron and hole carriers and are usually quite small, of the order of a few μV/K at room temperature and vanishing at low temperature. While superconductors obey overall electron-hole symmetry, spin-splitting of the quasiparticle density of states breaks electron-hole symmetry for each spin band, and in conjunction with the spin-dependent conductance of a superconductor-ferromagnet tunnel junction leads to thermoelectric effects [23–27]. The characteristic energy scale, the energy gap of the superconductor, is very small compared to the Fermi energy, and consequently, the thermoelectric effects are predicted to be large. The current through a tunnel junction in the presence of a voltage V and a temperature difference δT across the junction can be conveniently described in the linear regime by

$$I = gV + \eta \frac{\delta T}{\bar{T}}, \qquad (1)$$

where g is the conductance, $\bar{T}$ is the average temperature, and η describes the thermoelectric current. It is related to the Seebeck coefficient $S = -V/\delta T$ measured in an open circuit by $\eta = Sg\bar{T}$. Measuring the thermoelectric coefficient η is the main purpose of this work.

Our samples were prepared by e-beam lithography and the shadow evaporation technique. First, a thin superconducting (S) aluminum strip of thickness $t_{\mathrm{Al}} \approx 20$ nm was evaporated, which then was oxidized *in situ* to form a thin insulating (I) tunnel barrier. After that ferromagnetic (F) iron ($t_{\mathrm{Fe}} \approx 15$–$20$ nm) and normal-metal (N) copper wires ($t_{\mathrm{Cu}} \approx 50$ nm) were overlaid from different angles. In this Letter we present and compare results from three samples, two samples with ferromagnet-superconductor junctions (FIS1 and FIS2), and a nonmagnetic reference sample (NIS). Figure 1(a) shows a false-color scanning
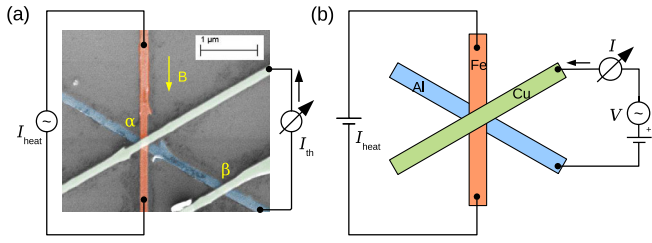
FIG. 1. (a) False-color scanning electron microscopy image of a region of sample FIS1 with the measurement configuration for the thermoelectric measurements. (b) Sketch of the measurement configuration for the conductance and heater calibration measurements.

electron microscopy image of a region of sample FIS1. The central part of the structure is a six-probe junction (α) consisting of a superconductor-ferromagnet tunnel contact overlaid with an additional copper wire. This design allows us to measure the current through the tunnel junction while simultaneously passing a heater current along the iron wire to create a temperature difference across the junction. In addition, there is a four-probe normal-metal junction (β), located at a distance $d \approx 1.5\ \mu$m from α. This junction is used for control experiments. Sample FIS2 has a slightly different layout (not shown) that avoids passing the heater current across the junction. As it turns out this had no effect on the results. The third sample (NIS) has the same layout as FIS1, with the iron wire replaced by a copper wire of a similar thickness. The measurement schemes are described below together with the results. Measurements were performed in a dilution refrigerator down to a base temperature of $T_0 = 50$ mK, with an in-plane magnetic field B applied parallel to the iron wire as indicated in Fig. 1(a). We denote the temperature of the refrigerator by T_0 to distinguish it from the electronic temperature of the sample throughout this Letter.

Before we describe the thermoelectric measurements, we first characterize the sample and calibrate the heater current. In Figs. 2(a) and 2(b) we show the differential conductance g of junction α of sample FIS1, measured by the standard low-frequency ac technique in the configuration shown in Fig. 1(b), without heater current. Figure 2(a) shows g as a function of bias voltage V for different magnetic fields B. In high fields the Zeeman splitting of the density of states is visible together with a broadening of the curves due to orbital pair breaking. To fit our data, we model the current using Eq. (2a) of Ref. [25]. We assume that the superconductor is at temperature $T_S = T$, and the ferromagnet is at temperature $T_F = T + \delta T$, with voltage V applied to the ferromagnet. This yields

$$I(T, \delta T, V) = \frac{G_T}{e} \int \left[N_0(E) + \frac{PN_z(E)}{2} \right]$$
$$\times [f_0(E - eV, T + \delta T) - f_0(E, T)]dE, \quad (2)$$
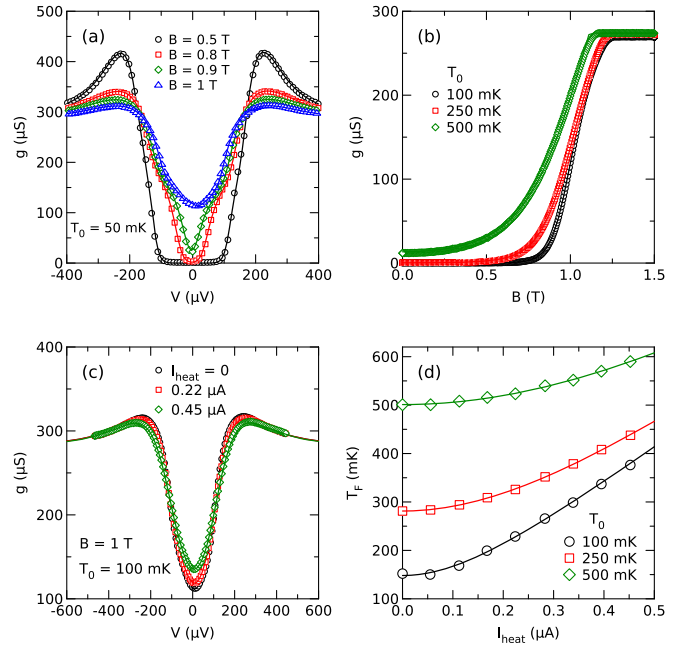
FIG. 2. (a) Differential conductance g of junction α of sample FIS1 as a function of bias V for different magnetic fields B. (b) Zero-bias conductance g as a function of magnetic field B for different base temperatures T_0. (c) Differential conductance g at fixed base temperature and magnetic field for different heater currents I_{heat}. (d) Temperature T_F of the ferromagnet as a function of I_{heat} for different T_0.

where G_T is the normal-state junction conductance, P is the spin polarization of the junction conductance, $e = -|e|$ is the charge of the electron, and f_0 is the Fermi function. Equation (2) includes the conductance ($V \neq 0$, $\delta T = 0$) and thermoelectric currents ($V = 0$, $\delta T \neq 0$) on an equal footing. The density of states factors are $N_0 = (N_+ + N_-)/2$ and $N_z = N_+ - N_-$, where $N_\pm$ are the densities of states for the two spin projections in the superconductor. N_+ and N_- were obtained from the standard model of high-field tunneling [36,37]. The factor PN_z is odd in energy, and gives rise to the observed thermoelectric effect. It is nonzero only in the presence of a Zeeman splitting of the density of states in combination with a spin-polarized junction conductance. Fits of our data based on Eq. (2) are shown as lines in Fig. 2(a) [38]. From these fits we extract the spin polarization $P \approx 0.08$. Because of the finite spin polarization P, there is a small but visible asymmetry of the conductance at high fields [43,44], with a higher conductance for electrons (negative bias) than holes (positive bias). In Fig. 2(b) we show g at zero bias as a function of the magnetic field B for three base temperatures T_0, together with fits to our model [38]. The fits of the conductance are used to establish the necessary sample parameters for modeling the thermoelectric results shown below.

We now turn to the heater calibration. In Fig. 2(c) we show the differential conductance g as a function of bias V at fixed temperature $T_0 = 100$ mK and magnetic field

$B = 1$ T for different dc heater currents I_{heat} [see Fig. 1(b) for the schematics]. Upon increasing I_{heat}, the conductance visibly broadens due to the increasing temperature T_F of the ferromagnet (the thermal broadening depends on T_F only and is independent of T_S). From the fits of the data we extract T_F as a function of I_{heat}, shown in Fig. 2(d) for three different base temperatures T_0.

To describe the heating of the junction as a function of current, we assume quasiequilibrium with negligible electron-phonon scattering, as appropriate for mesoscopic metal wires of about 10 μm length at sub-Kelvin temperatures [14]. In this case, the temperature at the junction (in the middle of the heater wire) is given by

$$T_F = \sqrt{T^2 + \frac{I_{\text{heat}}^2 R_{\text{heat}}^2}{4L_0}}, \qquad (3)$$

where R_{heat} is the resistance of the heater wire, $L_0 = \pi^2 k_B^2 / 3e^2$ is the Lorenz number, and T is the electronic base temperature in the absence of heating. In Fig. 2(d) we show fits of our data using Eq. (3). As can be seen, the fits show a good agreement with the data, and we use the fits for temperature calibration for the thermoelectric measurements described below. The electronic base temperature T is slightly increased over the cryostat base temperature T_0 at low temperatures, probably due to incomplete filtering of thermal noise from higher temperature stages of the cryostat. The fits yield $R_{\text{heat}} \approx 230$ Ω, smaller than the two-probe resistance of the iron wire, $R_{\text{Fe}} = 1350$ Ω. We attribute this to the fact that the thick copper wire acts as a cooling fin.

Superconductors are poor heat conductors at low temperature, and can therefore be easily heated. To check the impact of the heater current on the temperature T_S of the superconductor we performed additional control experiments on junction β. The quasiparticle energy relaxation length is typically a few 10 μm in aluminum at low temperatures [45], and we assume T_S to be nearly the same at contacts α and β. An increase of T_S affects the differential conductance g only indirectly by a small reduction of the pair potential Δ. In Fig. 3 we show data of sample FIS2, for which we made the most detailed measurements of T_S. Figure 3(a) shows the differential conductance g for different heater currents I_{heat} at fixed magnetic field $B = 1.3$ T and temperature $T_0 = 100$ mK. As can be seen, there is almost no change at small currents, and at larger currents, the gap is slightly reduced. The pair potential Δ obtained by fitting the data is plotted in Fig. 3(b) as a function of the heater current. The change of Δ is of the order of a few μeV for the largest applied current, with considerable scatter on this small scale. To reduce scatter, we averaged the data for two adjacent points and then inverted the self-consistent relation $\Delta(T + \delta T_S, B)$ to obtain δT_S (assuming $\delta T_S = 0$ for the first point). In Fig. 3(c) the resulting δT_S is shown as a
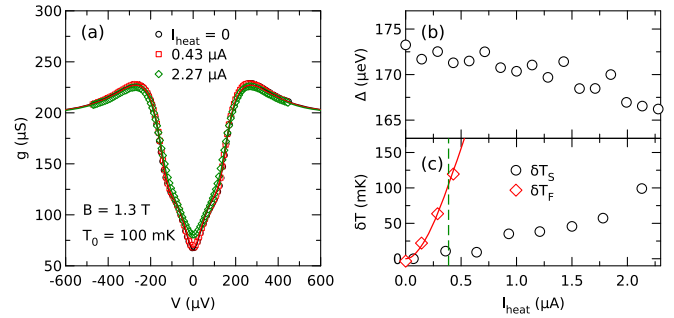
FIG. 3. (a) Differential conductance g of contact β of sample FIS2 at fixed magnetic field B and temperature T_0 for different heater currents I_{heat}. (b) Pair potential Δ as a function of I_{heat} obtained by fitting the differential conductance shown in (a). (c) Increase δT_S of the temperature of the superconductor as a function of I_{heat} extracted by inverting $\Delta(T_S)$, together with δT_F.

function of I_{heat}, together with δT_F. For thermal bias $\delta T_F < 100$ mK used in the thermoelectric experiments (indicated by the dashed line), we find $\delta T_S \lesssim 20$ mK, much smaller than δT_F. We conclude that most of the thermal bias actually drops across the junction.

Now we will focus on the main results of our work, the thermoelectric measurements. For these measurements, we applied an ac heater current, as shown schematically in Fig. 1(a). Since the heating power is proportional to I_{heat}^2, the thermal excitation appears on the second harmonic of the signal, and we detected the second harmonic of the resulting current I_{th} flowing into the superconductor. The heater current amplitude was typically chosen to yield a peak-to-peak thermal amplitude $\delta T_F = 100$ mK. In Fig. 4(a) we show the peak-to-peak amplitude of the thermoelectric current I_{th} as function of the magnetic field B at base temperature $T_0 = 100$ mK for sample FIS1. As expected, there is no signal at zero field, i.e., in the absence of Zeeman splitting. With increasing field a negative signal develops above $B = 0.5$ T and reaches a broad maximum around $B = 1$ T, and then goes back to zero as B approaches the critical field. The thermoelectric current is negative, as expected for our junction with a higher conductance for electrons than holes, as seen in Fig. 2(a). We also show theoretical calculations using Eq. (2) with the same parameters as for the fits of the conductance shown in Fig. 2(b). For the amplitude δT we chose two assumptions: the dashed line is calculated using $\delta T = \delta T_F = 100$ mK obtained from the calibration fit to Eq. (3), whereas the dash-dotted line is calculated using $\delta T = \delta T_F - \delta T_S \approx 80$ mK. The data lie in between both curves, and the best fit (solid line) is obtained for $\delta T = 86$ mK. The uncertainty in δT, which is reflected in the spread of the three model plots, is the main source of error in the determination of the thermoelectric coefficients [38].

In Fig. 4(b) we show the thermoelectric coefficient $\eta = I_{\text{th}} \bar{T} / \delta T$ for sample FIS1 as a function of the magnetic field B for different base temperatures T_0. Here, $\bar{T} = T + \delta T/2$, and we used δT from the best fits. For increasing
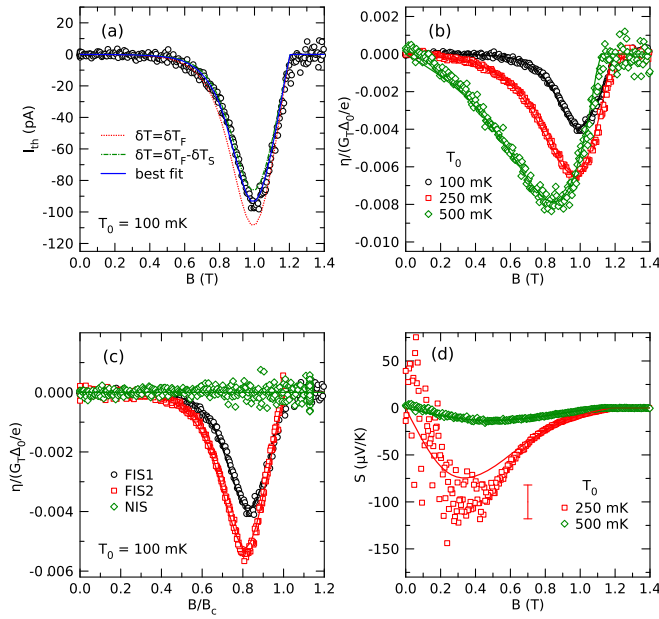
FIG. 4. (a) Thermoelectric current I_{th} as a function of magnetic field B at base temperature $T_0 = 100$ mK, together with theoretical calculations (see text). (b) Thermoelectric coefficient η of sample FIS1 for different temperatures T_0. (c) Thermoelectric coefficient η at $T_0 = 100$ mK for all three samples. (d) Seebeck coefficient S as a function of B calculated as described in the text. The error bar indicates the estimated error for the maximum at $T_0 = 250$ mK [38].

temperatures we see that both the magnitude and broadening of η increase, as expected from theory [25]. For $T_0 = 500$ mK, a sign reversal is visible at small fields. The sign of the thermoelectric current is determined by the relative sign of the Zeeman splitting and the spin polarization, and can reverse due to fringing fields. This effect has been observed in previous experiments on spin transport in Zeeman-split superconductors [6,8]. Figure 4(c) shows η as a function of the normalized field B/B_c for all samples at $T_0 = 100$ mK. The data are similar for both ferromagnetic samples FIS1 and FIS2. There is no signal for the nonmagnetic reference sample NIS, directly proving the spin-dependent origin of the effect. From the data and fits in Figs. 4(a)–4(c), we conclude that the data are in excellent qualitative and quantitative agreement with the theoretical predictions [25].

In Fig. 4(d) we finally show the Seebeck coefficient $S = \eta/(g\bar{T})$ inferred from our measurements as a function of the applied magnetic field B for sample FIS1. The data and fits of S were both calculated from the data and fits of η and g shown in Figs. 4(b) and 2(b). As can be seen, S shows a similar field dependence as η itself, however with a faster increase and maximum at smaller fields. The Seebeck coefficient is larger at lower temperature due to the freeze-out of the quasiparticle conductance. As a result, the scatter is also amplified, and the data for $T_0 = 100$ mK are unreliable and omitted from the plot. The increase of S

with decreasing T seems surprising, but theory actually predicts a nonmonotonic temperature dependence with an eventual drop to zero towards $T = 0$ [see Eq. (8) of Ref. [25]. For $T_0 = 250$ mK, the maximum value is $S \approx -100\ \mu V/K$. The error bar indicates the error due to the uncertainty of δT [38].

In conclusion, we have measured thermoelectric currents in superconductor-ferromagnet tunnel junctions at high magnetic fields. The results are in excellent agreement with recent theoretical predictions, and directly prove the coupling of spin and heat transport in high-field superconductors. The Seebeck coefficients inferred from the data can be as large as 100 μV/K, much larger than usually found in metal structures. The key ingredients for large thermoelectric effects in these structures are high spin polarization of the tunnel junction and well-resolved spin splitting of the density of states in the superconductor. Larger spin polarization can be achieved using spin-filter junctions [46,47], and Seebeck coefficients exceeding 1 mV/K seem feasible. Also, spin splitting has been observed in NbN with a critical temperature of about 16 K [48], and with GdN as the spin filter material [49] the temperature range above 4 K is accessible.

*Present address: Institute of Technical Physics, Karlsruhe Institute of Technology, 76021 Karlsruhe, Germany.
†detlef.beckmann@kit.edu

[1] R. S. Keizer, S. T. B. Goennenwein, T. M. Klapwijk, G. Miao, G. Xiao, and A. Gupta, Nature (London) **439**, 825 (2006).
[2] T. S. Khaire, M. A. Khasawneh, W. P. Pratt, and N. O. Birge, Phys. Rev. Lett. **104**, 137002 (2010).
[3] J. W. A. Robinson, J. D. S. Witt, and M. G. Blamire, Science **329**, 59 (2010).
[4] H. Yang, S.-H. Yang, S. Takahashi, S. Maekawa, and S. S. P. Parkin, Nat. Mater. **9**, 586 (2010).
[5] T. Wakamura, H. Akaike, Y. Omori, Y. Niimi, S. Takahashi, A. Fujimaki, S. Maekawa, and Y. Otani, Nat. Mater. **14**, 675 (2015).
[6] C. H. L. Quay, D. Chevallier, C. Bena, and M. Aprili, Nat. Phys. **9**, 84 (2013).
[7] F. Hübler, M. J. Wolf, D. Beckmann, and H. v. Löhneysen, Phys. Rev. Lett. **109**, 207001 (2012).
[8] M. J. Wolf, F. Hübler, S. Kolenda, H. v. Löhneysen, and D. Beckmann, Phys. Rev. B **87**, 024517 (2013).
[9] M. J. Wolf, C. Sürgers, G. Fischer, and D. Beckmann, Phys. Rev. B **90**, 144509 (2014).
[10] B. Li, G.-X. Miao, and J. S. Moodera, Phys. Rev. B **88**, 161105 (2013).
[11] C. H. L. Quay, M. Weideneder, Y. Chiffaudel, C. Strunk, and M. Aprili, Nat. Commun. **6**, 8660 (2015).
[12] M. Eschrig, Phys. Today **64**, No. 1, 43 (2011).
[13] J. Linder and J. W. A. Robinson, Nat. Phys. **11**, 307 (2015).

[14] F. Giazotto, T. T. Heikkilä, A. Luukanen, A. M. Savin, and J. P. Pekola, Rev. Mod. Phys. **78**, 217 (2006).

[15] J. T. Muhonen, M. Meschke, and J. P. Pekola, Rep. Prog. Phys. **75**, 046501 (2012).

[16] J. Eom, C.-J. Chien, and V. Chandrasekhar, Phys. Rev. Lett. **81**, 437 (1998).

[17] F. Giazotto and M. J. Martínez-Pérez, Nature (London) **492**, 401 (2012).

[18] M. José Martínez-Pérez and F. Giazotto, Nat. Commun. **5**, 3579 (2014).

[19] C. D. Shelly, E. A. Matrozova, and V. T. Petrashov, arXiv:1508.07249.

[20] A. Slachter, F. L. Bakker, J.-P. Adam, and B. J. van Wees, Nat. Phys. **6**, 879 (2010).

[21] J. Flipse, F. L. Bakker, A. Slachter, F. K. Dejene, and B. J. van Wees, Nat. Nanotechnol. **7**, 166 (2012).

[22] G. E. W. Bauer, E. Saitoh, and B. J. van Wees, Nat. Mater. **11**, 391 (2012).

[23] P. Machon, M. Eschrig, and W. Belzig, Phys. Rev. Lett. **110**, 047002 (2013).

[24] P. Machon, M. Eschrig, and W. Belzig, New J. Phys. **16**, 073002 (2014).

[25] A. Ozaeta, P. Virtanen, F. S. Bergeret, and T. T. Heikkilä, Phys. Rev. Lett. **112**, 057001 (2014).

[26] M. S. Kalenkov and A. D. Zaikin, Phys. Rev. B **90**, 134502 (2014).

[27] M. S. Kalenkov and A. D. Zaikin, Phys. Rev. B **91**, 064504 (2015).

[28] F. Giazotto, P. Solinas, A. Braggio, and F. S. Bergeret, Phys. Rev. Applied **4**, 044016 (2015).

[29] F. S. Bergeret and F. Giazotto, Phys. Rev. B **88**, 014515 (2013).

[30] F. Giazotto, J. W. A. Robinson, J. S. Moodera, and F. S. Bergeret, Appl. Phys. Lett. **105**, 062602 (2014).

[31] F. Giazotto, T. T. Heikkilä, and F. S. Bergeret, Phys. Rev. Lett. **114**, 067001 (2015).

[32] M. Silaev, P. Virtanen, F. S. Bergeret, and T. T. Heikkilä, Phys. Rev. Lett. **114**, 167002 (2015).

[33] I. V. Bobkova and A. M. Bobkov, JETP Lett. **101**, 118 (2015).

[34] T. Krishtop, M. Houzet, and J. S. Meyer, Phys. Rev. B **91**, 121407 (2015).

[35] I. V. Bobkova and A. M. Bobkov, Phys. Rev. B **93**, 024513 (2016).

[36] K. Maki, Prog. Theor. Phys. **32**, 29 (1964).

[37] R. Meservey, P. M. Tedrow, and R. C. Bruno, Phys. Rev. B **11**, 4224 (1975).

[38] See Supplemental Material at http://link.aps.org/supplemental/10.1103/PhysRevLett.116.097001, which includes Refs. [39–42], for details on fit procedures, sample parameters, and error estimates.

[39] J. A. X. Alexander, T. P. Orlando, D. Rainer, and P. M. Tedrow, Phys. Rev. B **31**, 5811 (1985).

[40] P. M. Tedrow and R. Meservey, Phys. Rev. B **7**, 318 (1973).

[41] M. Münzenberg and J. S. Moodera, Phys. Rev. B **70**, 060402 (2004).

[42] P. M. Tedrow, J. T. Kucera, D. Rainer, and T. P. Orlando, Phys. Rev. Lett. **52**, 1637 (1984).

[43] P. M. Tedrow and R. Meservey, Phys. Rev. Lett. **26**, 192 (1971).

[44] R. Meservey and P. M. Tedrow, Phys. Rep. **238**, 173 (1994).

[45] K. Y. Arutyunov, H.-P. Auraneva, and A. S. Vasenko, Phys. Rev. B **83**, 104509 (2011).

[46] X. Hao, J. S. Moodera, and R. Meservey, Phys. Rev. B **42**, 8235 (1990).

[47] G.-X. Miao and J. S. Moodera, Phys. Chem. Chem. Phys. **17**, 751 (2015).

[48] H. Yang, S.-H. Yang, C. Kaiser, and S. Parkin, Appl. Phys. Lett. **88**, 182501 (2006).

[49] K. Senapati, M. G. Blamire, and Z. H. Barber, Nat. Mater. **10**, 849 (2011).